Hybrid predictive control for aerial robotic physical interaction towards inspection operations

Author(s):
Darivianakis, Georgios; Alexis, Kostas; Burri, Michael; Siegwart, Roland

Publication date:
2014

Permanent link:
https://doi.org/10.3929/ethz-a-010089112

Originally published in:
https://doi.org/10.1109/ICRA.2014.6906589

Hybrid Predictive Control for Aerial Robotic Physical Interaction towards Inspection Operations

Georgios Darivianakis, Kostas Alexis, Michael Burri, and Roland Siegwart

***Abstract*— The challenge of aerial robotic physical interaction towards inspection of infrastructure facilities through contact is the main motivation of this paper. A hybrid model predictive control framework is proposed, based on which a typical quadrotor vehicle becomes capable of stable physical interaction, accurate trajectory tracking on environmental surfaces as well as force control with only minor structural adaptations. Convex optimization techniques enabled the explicit computation of such a controller which accounts for the dynamics in free–flight and during physical interaction, ensures the stability of the hybrid system as well as response optimality, while respecting system constraints and imposed logical rules. This control framework is further extended to include obstacle avoidance capabilities. Extensive experimental studies that included complex "aerial–writing" tasks, interaction with non–planar and textured surfaces and obstacle avoidance maneuvers, indicate the efficiency of the approach and the potential capabilities of such aerial robotic physically interacting operations.**

I. INTRODUCTION

Miniature Aerial Vehicles (MAVs) have proven to be a highly efficient class of systems with great potential on inspection operations. Utilizing vision, LiDARs or other sensing devices, MAVs are capable of executing complex remote aerial inspection tasks. However, infrastructure inspection operations are not limited to remote sensing but often require physical contact too. Due to this fact and further motivations, several research groups [1–4] have focused on addressing the problem of aerial physical interaction. This work proposes a control framework that provides advanced robotic physical interaction capabilities with only minor structural adaptations of the vehicle.

As shown in Figure 1, a typical quadrotor vehicle is utilized with the only mechanical adaptation being the integration of a simple rigid docking mechanism. The dynamics of the aerial robot are modeled during free–flight as well as during physical interaction and a global model is assembled employing the theory of hybrid automata and their equivalent translation to piecewise affine (PWA) systems. Based on the great breakthroughs in the field of convex optimization, the derived hybrid model becomes the basis for the computation of a powerful explicit hybrid model predictive control law (hybrid MPC). This controller provides a set of key features that are of critical importance for the field of aerial contact–based inspection and physical interaction in general. Most importantly, it ensures stable transitioning between free–flight and physical contact and achieves response optimality while satisfying the modeled system constraints and imposed mission–related logical rules. Consequently, accurate in–contact trajectory tracking is achieved along with force control capabilities. Furthermore, this control framework is extended to include means of obstacle avoidance. Being explicitly computed, it allows for fast real–time execution.

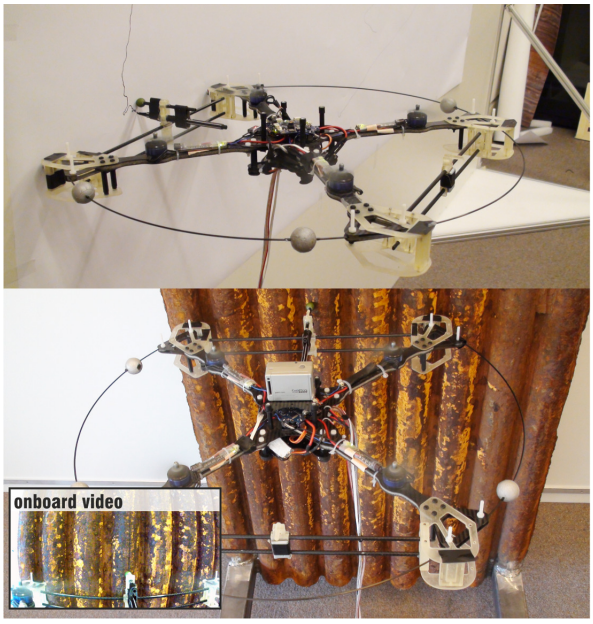

Fig. 1. Aerial robotic physical interaction experiments.

The properties of the controlled system were evaluated experimentally. Mounting a marker on the vehicle, a wide set of "aerial–writing" operations were conducted in order to evaluate the capabilities of aerial physical interaction and inspection through contact. Such an "aerial–writing" task may be considered similar to that of non–destructive testing (NDT) of infrastructure using ultrasound probes. Despite the constraints imposed from the environment and the underactuated nature of the vehicle dynamics, sufficiently accurate in–contact trajectory tracking and force control was achieved. Moreover, the capacity for achieving smooth approaching and docking maneuvers even subject to temporal faults of the position localization subsystem was evaluated. Finally, the capabilities of obstacle avoidance are presented.

This paper is structured as follows. In Section II, the hybrid model of the system dynamics is presented, followed by the development of the hybrid model predictive controller

This work was supported by the European project ICARUS funded by the European Commision under the 7th Framework Programm.

All authors are with the Autonomous Systems Lab at ETH Zurich, Tannenstrasse 3, 8092 Zurich, Switzerland. email: konstantinos.alexis@mavt.ethz.ch

in Section III. Extended experimental studies are presented in Section IV, while conclusions are drawn in Section V.

II. HYBRID MODELING

The utilized "ASLquad" is a quadrotor aerial robot that adopts an in–house airframe development, the electronic and actuation components of an AscTec Hummingbird and a modular software framework. The airframe has an arm length $l_a = 0.3$m and A docking mechanism has been mounted on its front and back side to ensure a safe physical interaction. Such a mechanism corresponds to the only required structural modification to any multirotor, so that similar aerial physical interaction tasks become possible. On the front side, a marker is mounted so that writing tasks are executed and visually verified. The overall mass is $m = 0.65$kg.

A. Attitude Dynamics Identification

An attitude controller was already implemented for this vehicle. The choice of not designing a specialized attitude controller was motivated by the fact that nowadays, a huge market of multirotors and other unmanned rotorcrafts exists with such a low–level controller already integrated. As long as physical interaction tasks can be executed safely and accurately by only adapting the high–level controller, the choise of redesigning the attitude loop was considered unjustified. However, a model of the closed–loop attitude dynamics had to be derived. Using grey–box frequency domain methods, second order models of the roll, pitch and yaw dynamics are computed. The employed grey–box structures take the following form:

$$\begin{bmatrix} \dot{\lambda} \\ \ddot{\lambda} \end{bmatrix} = \begin{bmatrix} 0 & 1 \\ -b_{\dot{\lambda},\lambda} & -b_{\dot{\lambda},\dot{\lambda}} \end{bmatrix} \begin{bmatrix} \lambda \\ \dot{\lambda} \end{bmatrix} + \begin{bmatrix} 0 \\ c_{\dot{\lambda},\lambda^r} \end{bmatrix} \lambda^r \tag{1}$$

where λ refers to each one of the roll, pitch, yaw angles ϕ, θ, ψ and λ^r to their reference signals.

B. Hybrid Physical Interaction Dynamics

In order to develop an aerial robot capable of active physical interaction with its environment, a modeling methodology that captures the system dynamics during all the modes of its operation has to be employed. Since the collision dynamics are expressed in time scales that are orders of magnitude smaller than those of the vehicle motion dynamics, the system is considered to change mode instantaneously. Therefore, the powerful theoretical tools of hybrid systems are utilized to develop a global model of such an aerial robot during free–flight as well as physical interaction.

Extending the approaches presented in [2, 3], a hybrid automaton that captures the behavior of the system in all of its modes as well as the event mechanism that triggers the mode transitions is derived and becomes the basis for model–based control synthesis. The problem is decoupled in three loops, namely, a) the forward–motion longitudinal dynamics that are constrained during physical interaction, b) the lateral and c) the altitude dynamics which are both affected by friction once contact is established. Correspondingly, three hybrid automata are formulated. Figure 2 presents the structure of each of these hybrid automata, its modes $\mathbf{Q} = \{FF, PI\}$ and event mechanism as well as the utilized coordinate frame.

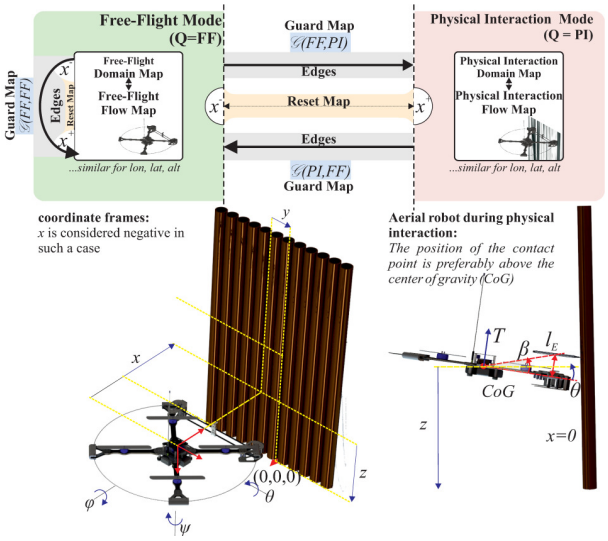

Fig. 2. The structure of the free–flight and physical interaction hybrid automaton and the employed coordinate frame.

Each of the three hybrid automata is formulated along the lines of [5]. Either in free–flight or during physical interaction, the inputs of each of the longitudinal, lateral and altitude subsystems belongs to a bounded set $\mathbf{u}_\xi \in \mathscr{U}_\xi$, $\xi \rightarrow lon, lat, alt$. Similarly, the states of each subsystem may be constrained in a bounded set $\mathscr{S}_\xi$ once contact is established. Consequently, a *Domain Map* is defined for the continuous states of each of the modes of every hybrid automaton:

$$\begin{aligned} \mathscr{D}_\xi(FF) &: \mathbb{R}^4 \times \mathscr{U}_\xi \\ \mathscr{D}_\xi(PI) &: \mathscr{S}_\xi^4 \times \mathscr{U}_\xi \end{aligned} \tag{2}$$

A locally Lipschitz *Flow Map* $f(\mathbf{x}_\xi, \mathscr{D}_\xi)$ acts on these domain maps and describes the continuous evolution of the states for every operative mode. Each of the flow maps consists of two components $f(\mathbf{x}_\xi, \mathscr{D}_\xi(FF))$, $f(\mathbf{x}_\xi, \mathscr{D}_\xi(PI))$ for the free–flight and physical interaction modes respectively. The following state–space representations describe the evolution of the longitudinal dynamics:

$$\begin{cases} f(\mathbf{x}_{lon}, \mathscr{D}_{lon}(FF)) : \dot{\mathbf{x}}_{lon} = \mathbf{A}_{lon}^{FF}\mathbf{x}_{lon} + \mathbf{B}_{lon}^{FF}\mathbf{u}_{lon} \\ f(\mathbf{x}_{lon}, \mathscr{D}_{lon}(PI)) : \dot{\mathbf{x}}_{lon} = \mathbf{A}_{lon}^{PI}\mathbf{x}_{lon} + \mathbf{B}_{lon}^{PI}\mathbf{u}_{lon} + \mathbf{G}_{lon}^{PI}F_E \end{cases} \tag{3}$$
$$\mathbf{x}_{lon} = [x, \dot{x}, \theta, \dot{\theta}]^T,\ \mathbf{y}_{lon} = [x, \dot{x}, \theta, \dot{\theta}, F_x]^T,\ \mathbf{u}_{lon} = \theta^r$$

where,

$$\mathbf{A}_{lon}^{FF} = \begin{bmatrix} 0 & 1 & 0 & 0 \\ 0 & -\lambda_{lon}^{FF} & -g & 0 \\ 0 & 0 & 0 & 1 \\ 0 & 0 & -b_{\dot{\theta},\theta} & -b_{\dot{\theta},\dot{\theta}} \end{bmatrix},\ \mathbf{B}_{lon}^{FF} = \begin{bmatrix} 0 \\ 0 \\ 0 \\ c_{\dot{\theta},\theta^r} \end{bmatrix}$$

$$\mathbf{A}_{lon}^{PI} = \begin{bmatrix} 0 & 1 & 0 & 0 \\ 0 & 0 & 0 & 0 \\ 0 & 0 & 0 & 1 \\ 0 & 0 & -b_{\dot{\theta},\theta} & -b_{\dot{\theta},\dot{\theta}} \end{bmatrix},\ \mathbf{B}_{lon}^{PI} = \begin{bmatrix} 0 \\ 0 \\ 0 \\ c_{\dot{\theta},\theta^r} \end{bmatrix},\ \mathbf{G}_{lon}^{PI} = \begin{bmatrix} 0 \\ 0 \\ 0 \\ l_E \end{bmatrix}$$

and F_E is the force exerted from the environment and under rigid–body assumptions is equal and opposite to the projected

force on the x–axis ($F_E = -F_x$, $F_x = -T\sin\theta$) during stable contact. As shown, the flow map during physical interaction encodes the fact that the system is physically constrained in the forward direction. The lever arm $l_E = l_a \sin(\beta - \theta)$, ($\beta = 0.14$rad), is approximated for $\theta = -0.035$rad which corresponds to a typical docking angle, while the longitudinal position x is defined as the distance of the vehicle CoG to the closest surface of the environment minus the distance of the CoG to the contact point and is considered negative in free–flight and zero during contact ($x \in (-\infty, 0]$). The output vector is set as $y_{lon} = [x, \dot{x}, \theta, \dot{\theta}, F_x]^T$, $F_x \approx -mg\theta$ in order to enable output tracking with force control capabilities. The lateral motion flow map takes the following form:

$$\begin{cases} f(\mathbf{x}_{lat}, \mathscr{D}_{lat}(FF)) & : \quad \dot{\mathbf{x}}_{lat} = \mathbf{A}_{lat}^{FF}\mathbf{x}_{lat} + \mathbf{B}_{lat}^{FF}\mathbf{u}_{lat} \\ f(\mathbf{x}_{lat}, \mathscr{D}_{lat}(PI)) & : \quad \dot{\mathbf{x}}_{lat} = \mathbf{A}_{lat}^{PI}\mathbf{x}_{lat} + \mathbf{B}_{lat}^{PI}\mathbf{u}_{lat} \\ & \mathbf{x}_{lat} = [y, \dot{y}, \phi, \dot{\phi}]^T,\ \mathbf{y}_{lat} = \mathbf{x}_{lat},\ \mathbf{u}_{lat} = \phi^r \end{cases} \tag{4}$$

where,

$$\mathbf{A}_{lat}^{FF} = \begin{bmatrix} 0 & 1 & 0 & 0 \\ 0 & -\lambda_{lat}^{FF} & g & 0 \\ 0 & 0 & 0 & 1 \\ 0 & 0 & -b_{\dot{\phi},\phi} & -b_{\dot{\phi},\dot{\phi}} \end{bmatrix},\ \mathbf{B}_{lat}^{FF} = \begin{bmatrix} 0 \\ 0 \\ 0 \\ c_{\dot{\phi},\phi^r} \end{bmatrix}$$

$$\mathbf{A}_{lat}^{PI} = \begin{bmatrix} 0 & 1 & 0 & 0 \\ 0 & -\lambda_{lat}^{PI} & g & 0 \\ 0 & 0 & 0 & 1 \\ 0 & 0 & -b_{\dot{\phi},\phi} & -b_{\dot{\phi},\dot{\phi}} \end{bmatrix},\ \mathbf{B}_{lat}^{PI} = \begin{bmatrix} 0 \\ 0 \\ 0 \\ c_{\dot{\phi},\phi^r} \end{bmatrix}$$

As shown the flow map during physical interaction accounts for the viscous friction effects through the adapted damping coefficient λ_{lat}^{PI}. Similarly, for the altitude subsystem:

$$\begin{cases} f(\mathbf{x}_{alt}, \mathscr{D}_{alt}(FF)) & : \quad \dot{\mathbf{x}}_{alt} = \mathbf{A}_{alt}^{FF}\mathbf{x}_{alt} + \mathbf{B}_{alt}^{FF}\mathbf{u}_{alt} \\ f(\mathbf{x}_{alt}, \mathscr{D}_{alt}(PI)) & : \quad \dot{\mathbf{x}}_{alt} = \mathbf{A}_{alt}^{PI}\mathbf{x}_{alt} + \mathbf{B}_{alt}^{PI}\mathbf{u}_{alt} \\ & \mathbf{x}_{alt} = [z, \dot{z}]^T,\ \mathbf{y}_{alt} = \mathbf{x}_{alt},\ \mathbf{u}_{alt} = T^r \end{cases} \tag{5}$$

where,

$$\mathbf{A}_{alt}^{FF} = \begin{bmatrix} 0 & 1 \\ 0 & -\lambda_{alt}^{FF} \end{bmatrix},\ \mathbf{B}_{alt}^{FF} = \begin{bmatrix} 0 \\ -\frac{1}{m} \end{bmatrix}$$

$$\mathbf{A}_{alt}^{PI} = \begin{bmatrix} 0 & 1 \\ 0 & -\lambda_{alt}^{PI} \end{bmatrix},\ \mathbf{B}_{alt}^{PI} = \begin{bmatrix} 0 \\ -\frac{1}{m} \end{bmatrix}$$

and T^r is the reference thrust signal. Again the adapted λ_{alt}^{PI} captures the effects of viscous friction.

The possible mode switchings are represented using the *Set of Edges* $\mathscr{E}$ as visualized in Figure 2. Since the vehicle may encounter elastic collisions, a rebound loop is added to the hybrid system $\{FF, FF\}$. The logic that governs the mode switchings, is encoded in the *Guard Map* $\mathscr{G}$ (Table I) which identifies the set $\mathscr{G}(q_i, q_j)$ to which the outputs of the system have to belong so that transition from the mode $q_i \in \mathbf{Q}$ to $q_j \in \mathbf{Q}$ may occur. By integrating tactile sensors and combining their data with the state variables, a robust contact detection strategy is engineered. For the lateral and altitude hybrid automata, an auxiliary boolean state is added and switches from 0 to 1 based on the aforementioned longitudinal guard maps in order to trigger mode switching. Value $\Delta\dot{x}^{\min} \to 0^+$ is a close to zero tunable threshold.

TABLE I
GUARD MAPS MODE SWITCHING LOGIC

	$\dot{x}$	s
$\mathscr{G}(FF,FF)$	$\dot{x}^+\dot{x}^- < 0,\ \lvert\dot{x}\rvert \geq \Delta\dot{x}^{\min}$	0 or 1
$\mathscr{G}(FF,PI)$	$\dot{x}^+\dot{x}^- \leq 0,\ \lvert\dot{x}\rvert \leq \Delta\dot{x}^{\min}$	$s = 1 \Rightarrow x = 0$
$\mathscr{G}(PI,FF)$	$\lvert\dot{x}\rvert \geq \dot{x}^{\min}$	$s = 0 \Rightarrow x < 0$

Finally, for completeness and simulation reasons, a *Reset Map* $\mathscr{R}$ is formulated for each hybrid automaton and describes, for every edge $(\{FF,FF\}, \{FF,PI\}, \{PI,FF\})$, the values to which the continuous states $\mathbf{x}_\xi$ are set during a mode transition. This reset map encodes the jump on the attitude rate and velocity of the vehicle in case of elastic collisions and follows the methodology presented in [6].

These hybrid automata represent a global model of the ASLquad during free–flight and physical interaction. Their implementation was achieved using the HYbrid System DEscription Language (HYSDEL) 3.0 [7] which provides a rapid prototyping framework integrated with MATLAB® and the Multiparametric Toolbox (MPT) 3.0 [8].

While hybrid automata provide an intuitive way for modeling, piecewise affine systems are more powerful for numerical control computation. Different hybrid systems representations are however translatable from one to the other with equivalence, in the sense that the same input sequences will lead to identical state trajectories. The equivalent PWA system takes the following form in discrete time:

$$\begin{aligned} \mathbf{x}_\xi(k+1) &= \mathbf{A}_{i(k)}^{\xi}\mathbf{x}_\xi(k) + \mathbf{B}_{i(k)}^{\xi}\mathbf{u}_\xi(k) + \mathbf{f}_{i(k)}^{\xi} \\ \mathbf{y}_\xi(k) &= \mathbf{C}_{i(k)}^{\xi}\mathbf{x}_\xi(k) + \mathbf{D}_{i(k)}^{\xi}\mathbf{u}_\xi(k) \end{aligned} \tag{6}$$

where $i(k)$ indicates which hybrid mode (PWA model) is active and the switching rule is now represented in a matrix inequalities form based on the states and inputs vectors:

$$\begin{aligned} \mathbf{H}_{i(k)}^{\xi}\mathbf{x}_\xi(k) + \mathbf{J}_{i(k)}^{\xi}\mathbf{u}_\xi(k) &\leq \mathbf{K}_{i(k)}^{\xi} \\ \tilde{\mathbf{H}}_{i(k)}^{\xi}\mathbf{x}_\xi(k) + \tilde{\mathbf{J}}_{i(k)}^{\xi}\mathbf{u}_\xi(k) &< \tilde{\mathbf{K}}_{i(k)}^{\xi} \end{aligned} \tag{7}$$

where the matrices $\mathbf{A}_{i(k)}^{\xi}$, $\mathbf{B}_{i(k)}^{\xi}$, $\mathbf{f}_{i(k)}^{\xi}$, $\mathbf{C}_{i(k)}^{\xi}$, $\mathbf{D}_{i(k)}^{\xi}$, $\mathbf{H}_{i(k)}^{\xi}$, $\mathbf{J}_{i(k)}^{\xi}$, $\mathbf{K}_{i(k)}^{\xi}$, $\tilde{\mathbf{H}}_{i(k)}^{\xi}$, $\tilde{\mathbf{J}}_{i(k)}^{\xi}$, $\tilde{\mathbf{K}}_{i(k)}^{\xi}$ are constant and have suitable dimensions, $i(k) = 1, \ldots, \mu$, where μ is the number of the PWA systems required to express the hybrid system ($\mu = 2$).

III. HYBRID MODEL PREDICTIVE CONTROL

The proposed control law exceeds the classical synthesis of MPC–based autopilots [9–12] and provides a set of key features for aerial robotic physical interaction operations. Utilizing the concept of receding horizon control over the hybrid model of the vehicle, it ensures its global stability as well as response optimality, while it also makes use of recent advancements in the field of convex optimization to provide a flexible framework that can incorporate artificially imposed mission–related logical rules together with the system state and input constraints. Finally, obstacle avoidance capabilities are incorporated in the same framework. MPT and YALMIP [13] are the main computational tools that enabled the design and explicit computation of such a controller.

A. State and Input Constraints

The following, state and input constraints are imposed in the optimization process in order to enforce the vehicle's operation in a safe subset of its flight envelope:

$$\begin{bmatrix}\mathbf{I}_{3\times3} & \mathbf{0}_{3\times3}\\ \mathbf{0}_{3\times3} & -\mathbf{I}_{3\times3}\end{bmatrix}\begin{bmatrix}\dot{x}\\ \theta\\ \theta^r\\ \dot{x}\\ \theta\\ \theta^r\end{bmatrix} \leq \begin{bmatrix}1.5\text{m/s}\\ \pi/4\text{rad}\\ \pi/4\text{rad}\\ 1.5\text{m/s}\\ \pi/4\text{rad}\\ \pi/4\text{rad}\end{bmatrix} \tag{8}$$

$$\begin{bmatrix}\mathbf{I}_{3\times3} & \mathbf{0}_{3\times3}\\ \mathbf{0}_{3\times3} & -\mathbf{I}_{3\times3}\end{bmatrix}\begin{bmatrix}\dot{y}\\ \phi\\ \phi^r\\ \dot{y}\\ \phi\\ \phi^r\end{bmatrix} \leq \begin{bmatrix}1.5\text{m/s}\\ \pi/4\text{rad}\\ \pi/4\text{rad}\\ 1.5\text{m/s}\\ \pi/4\text{rad}\\ \pi/4\text{rad}\end{bmatrix} \tag{9}$$

$$\begin{bmatrix}\mathbf{I}_{2\times2} & \mathbf{0}_{2\times2}\\ \mathbf{0}_{2\times2} & -\mathbf{I}_{2\times2}\end{bmatrix}\begin{bmatrix}\dot{z}\\ T^r\\ \dot{z}\\ T^r\end{bmatrix} \leq \begin{bmatrix}1.5\text{m/s}\\ 5\text{N}\\ 1.5\text{m/s}\\ 5\text{N}\end{bmatrix} \tag{10}$$

B. Imposed Logical Rules

Consequently, a second class of constraints that encode mission–related logical rules are also imposed. Although not captured from simple rigid body modeling, the vehicle has to apply at least a minimum force in order to retain contact due to the aerodynamic turbulence that occasionally creates repelling forces. Correspondingly, a safety constraint that enforces a minimum force threshold is imposed during physical interaction. Moreover, to prevent the vehicle from tipping over the wall due to the external moments, a tight hard constraint on the maximum pitch angle is imposed during contact. These logical rules take the following form:

$$\textbf{IF}\ \ contact \qquad \textbf{THEN} \qquad F_x \geq 0.2\text{N} \tag{11}$$

$$\textbf{IF}\ \ contact \qquad \textbf{THEN} \qquad \theta \leq \pi/12\text{rad} \tag{12}$$

YALMIP enables the incorporation of these non–convex logical rules in the optimization.

C. Control Computation

Provided the PWA representations of the hybrid systems as in (6),(7) as well as the constraints (8),(9),(10) and the logical rules (11), (12) three hybrid predictive controllers are computed in a multiparametric fashion [8, 14]. Using a quadratic norm as a metric of optimality and adding terminal set constraints, the hybrid predictive controller, for a prediction horizon N, consists of computing the optimal control sequence $\mathbf{U}_\xi^\mathbf{N} = [u_\xi(0),...,u_\xi(N-1)]$ that minimizes the following objective:

$$\begin{aligned}\mathbf{J}(x_{\xi,0},U_\xi^N) \quad = \quad & \min_{U_\xi^N}\{\mathbf{x}_{\xi,N}^T\mathbf{P}_{M\times M}\mathbf{x}_{\xi,N}+ \\ & \sum_{k=0}^{N-1}\mathbf{x}_{\xi,k}^T\mathbf{Q}_{M\times M}\mathbf{x}_{\xi,k}+\mathbf{u}_{\xi,k}^T\mathbf{R}_{L\times L}\mathbf{u}_{\xi,k}\} \\ s.t. \quad & \text{equation } (6),(7),[(8)/(9)/(10)],\ [(11),(12)]_{\xi\rightarrow lon} \\ & \mathbf{x}_{\xi,N}\in T_{set}\end{aligned} \tag{13}$$

where $\mathbf{P}_{M\times M}\succeq\mathbf{0}$, $\mathbf{Q}_{M\times M}\succeq\mathbf{0}$, $\mathbf{R}_{L\times L}\succeq\mathbf{0}$ are the weighting matrices of the terminal state, of the states and the manipulated variables respectively and T_{set} is the terminal set which is specified as the LQR terminal set in order to guarantee stability properties [14]. For each subsystem, such a hybrid MPC is computed based on state feedback. However, for the purposes of varying force reference, the aforementioned objective is reformulated in output feedback form.

D. Obstacle Avoidance

The proposed control framework may also be extended to provide obstacle avoidance capabilities by coupling the three hybrid automata, modifying the objective function and adding polyhedric constraints. In an infrastructure inspection scenario it is very likely that some knowledge of the main structure is available a priori, which then allows modeling of most of the obstacles in the workspace. Let $\mathscr{P}_w$ be a polyhedron that describes the total workspace of the robot, $\mathscr{P}_o^1,\mathscr{P}_o^2,...,\mathscr{P}_o^p$ polyhedra that enclose the known obstacles and also provide additional thresholds to account for the vehicle dimensions and some further safety bounds that allow limited penetration. The "safe" robot workspace is defined as the Pontryagin difference $\mathscr{P}_s=\mathscr{P}_w\setminus\{\mathscr{P}_o^1,\mathscr{P}_o^2,...,\mathscr{P}_o^p\}$. In order to enforce operation within $\mathscr{P}_s$, the following adaptation in the optimization problem is required:

$$\begin{aligned}\min_{U_\sigma^N} \quad & \mathbf{J}(x_{\sigma,0},U_\sigma^N) \\ \text{s.t.} \quad & [x,\ y,\ z]\in\mathscr{P}_s \\ & \text{equation } (6),(7),(8),(9),(10),(11),(12)\end{aligned} \tag{14}$$

where σ indicates that the coupled 3D hybrid automaton is used. Despite this problem is of increased complexity, once an explicit solution is computed, its real–time implementation is very efficient. It is noted that this obstacle avoidance strategy is not proposed in order to substitute the need for proper trajectory generation but rather as a last resort mechanism that ensures the system safety at the control level.

E. Explicit Implementation

One additional important property of the proposed control strategy is its explicit character. This is a result of the fact that the control action takes a piecewise affine form [15]:

$$\mathbf{u}_\xi(k) \quad = \quad \mathbf{F}_\xi^r\mathbf{x}_\xi(k)+\mathbf{G}_\xi^r,\ \text{if } \mathbf{x}_\xi(k)\in\Pi_\xi^r \tag{15}$$

where Π_ξ^i, $\xi\rightarrow lon,lat,alt$ or σ, $r=1,...,N_\xi^r$ are the regions of the receding horizon control strategy. The r–th control law is valid if the state vector $\mathbf{x}_\xi(k)$ is contained in a convex polyhedral region $\Pi_\xi^r=\{\mathbf{x}_\xi(k)\ |\mathbf{H}_\xi^r\mathbf{x}_\xi(k)\leq\mathbf{K}_\xi^r\}$ computed and described in h–representation during the explicit controller derivation [16]. The controller is equivalently translated to a mapping between feedback gains and affine terms $\mathbf{F}_\xi^r,\mathbf{G}_\xi^r$ and corresponding polyhedric regions Π_ξ^r. This explicit controller is equivalent to its online counterpart in the sense that for identical state trajectories, both produce the same control actions, and therefore share the same stabilizing and optimality properties. This fact enables the seamless real–time implementation of this controller. In the framework of this work, the real time code is described in Algorithm 1 and corresponds to an extension of the table traversal algorithm [16] that also supports multiple inputs.

Finally, in order to compensate for the possibly rotated yaw angle (ψ), the derived θ^r,ϕ^r reference signals are rotated accordingly.

Algorithm 1: Extended Sequential Table Traversal

Data: ***Regions***: H^r, K^r ***Regions feedback laws***: F^r, G^r, ***Regions Cost Matrices***: Q_r,f_r,g_r, ***Number of regions***: N^r, ***Input Penalization Matrix***: R_p, ***State*** : $x(k)$,***Previous Optimal Control input***: u_{prev}
Result: Explicit Hybrid MPC control input $u_0^*(x(k))$

$J_{min} \leftarrow +\infty$
$u_{opt} \leftarrow u_{prev}$
for $r = 1,...,N_r$ **do**
  if $H^r x_k \leq K^r$ **then**
    $J_r \leftarrow x(k)^T Q_r x(k) + f_r^T x(k) + g_r$; /* region cost */
    $u_r \leftarrow F^r x(k) + G^r$; /* region control input */
    if $J_r < J_{min}$ **then**
      $J_{min} \leftarrow J_r$;
      $u_{opt} \leftarrow u_r$;
    else if $J_r = J_{min}$ **then**
      if $u_r^T R_p u_r \leq u_{opt}^T R_p u_{opt}$ **then**
        $J_{min} \leftarrow J_r$;
        $u_{opt} \leftarrow u_r$;
      end
    end
  end
end
$u_0^*(x(k)) = u_{opt}$;

IV. EXPERIMENTAL EVALUATION

The efficiency of the proposed control framework was experimentally evaluated. Mounting a marker on the vehicle, a wide set of "aerial–writing" tasks were performed. Such tasks assess the capabilities of aerial contact–based inspection at the control level. Measurements of the thickness of power plant boiler pipes using ultrasound probes corresponds to an indicative example of such applications. Three sets of experiments were conducted, namely a) complex "aerial–writing", b) sliding on a real segment of boiler pipes also subject to temporal sensor faults and c) obstacle avoidance and docking. In all the conducted experiments position feedback was provided by a Vicon motion capture system, while the onboard inertial measurement unit provided the attitude estimates. The sampling time was set to $T_s = 0.02$s and $N = 10$. The x reference is always set 5cm behind the environmental surface.

Figure 3 depicts an inspection maneuver that "scans" a prespecified area on a wall with the reference precomputed offline. This, essentially imitates a mission of inspecting the walls of industrial facilities, in order to detect potential damages or developing hazards.

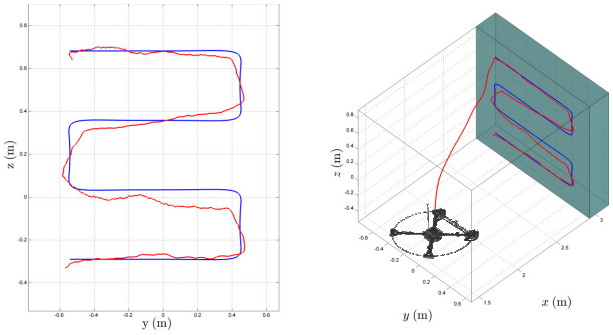

Fig. 3. Aerial writing experiment, executing a wall inspection through contact path. A recording of this response is available at the video file.

Subsequently, the vehicle was commanded to write a word, and specifically to write "ASL" (acronym of the Autonomous Systems Lab at ETH Zurich). The derived results, shown in Figure 4, present high accuracy compared to the challenging nature of the reference path, the underactuated dynamics of the vehicle and its limited force generation mechanism.

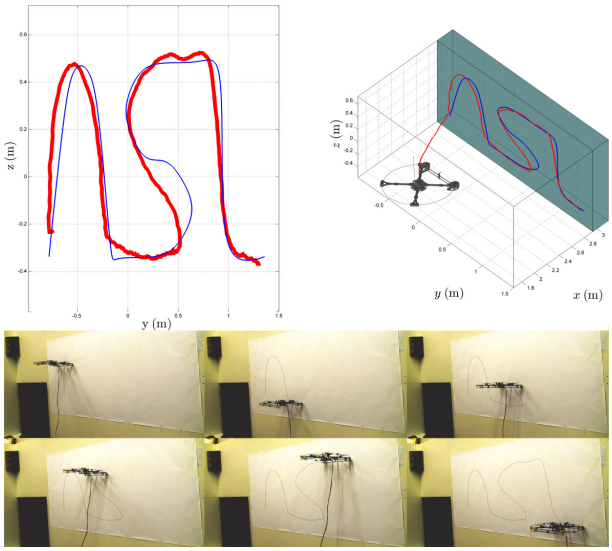

Fig. 4. Aerial writing of the Autonomous Systems Lab acronym (ASL). A recording of this response is available at the video file.

The next test–case evaluates the physical interaction capabilities on non–planar textured surfaces, as it can be expected in industrial inspection operations. As shown in Figure 5, the robot is commanded to dock and "write" a vertical line on a segment of a real power plant boiler pipe–wall.

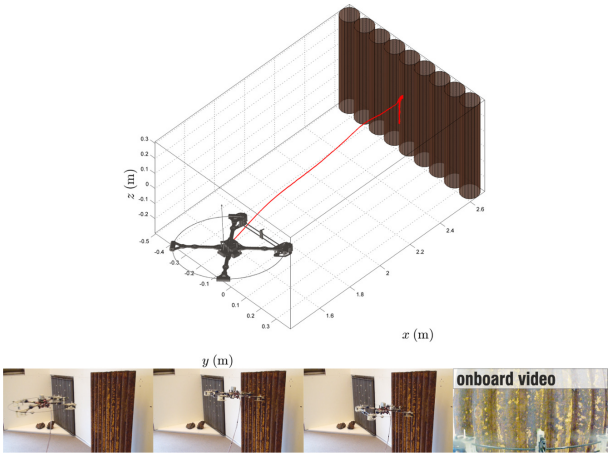

Fig. 5. Vertical sliding on a segment of a real boiler pipe–wall. A video recording of this response is available at the supplementary video file.

During real inspection operations, it may be expected that the position localization subsystem may encounter temporal faults. Such a situation becomes even more challenging if it happens during a docking maneuver. Towards providing a last resort safety mechanism, Figure 6 depicts that a smooth docking maneuver can still be achieved as long as a model

of sufficient fidelity is available. As shown, for the last 0.4m, the position feedback was based only on forward simulation of the identified dynamics, while once contact is detected the ground truth data were again provided to the system. As illustrated, in such an experiment, the maximum errors are small and the maneuver remains practically unaffected.

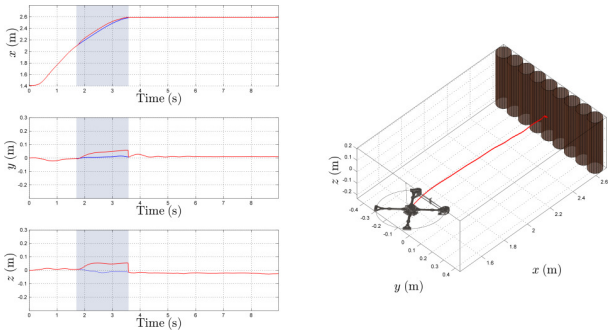

Fig. 6. Docking maneuver in case of position information loss by relying only on forward simulation of the identified models.

Finally, the obstacle avoidance capabilities were evaluated and the results are depicted in Figure 7. With prior knowledge of the obstacle position and dimensions, a bounding polyhedron $\mathscr{P}_o$, is defined and the controller described in Subsection III-D is applied. As demonstrated, a last resort obstacle avoidance mechanism is achieved and ensures the safety of the system.

V. CONCLUSIONS AND FUTURE WORK

A hybrid model predictive control framework that handles the problem of aerial physical interaction and inspection through contact with only minor structural adaptations of the aerial vehicle is proposed. Employing hybrid systems approaches, a global model of the system dynamics in free–flight as well as during physical interaction is derived and becomes the basis for model–based control. The proposed controller ensures the stability of the system and achieves optimal responses while satisfying constraints, imposed logical rules and avoiding obstacles. The efficiency of the proposed method was evaluted using extensive experimental studies that included "aerial–writing" tasks, non–planar and textured surfaces inspection and obstacle avoidance.

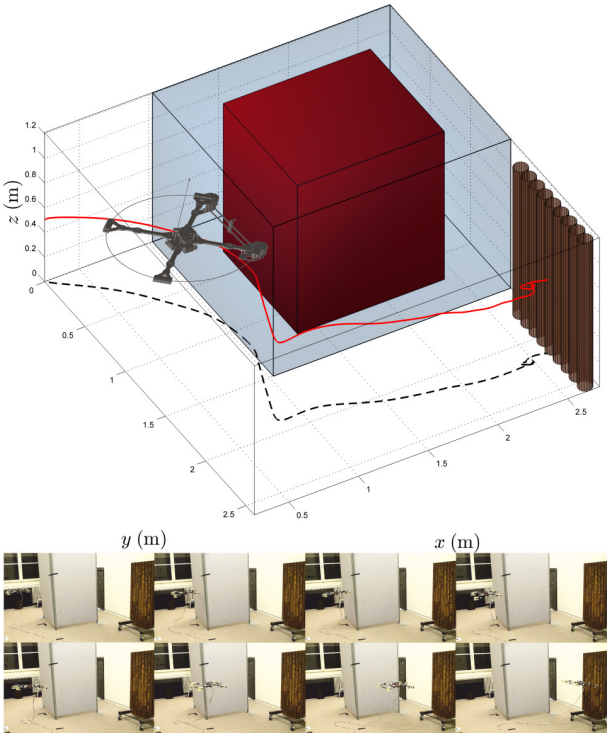

Fig. 7. Experiment presenting the obstacle avoidance capabilities of the proposed model predictive controller. The guarding (transparent) polyhedron $\mathscr{P}_o$ is larger than the real obstacle to account for the quadrotor size and provide safety thresholds. As shown rapid safety action takes place once short intervention to the guarding polyhedron is detected. A video recording of this response is available at the supplementary video file.

REFERENCES

[1] D. Mellinger, M. Shomin, N. Michael, and V. Kumar, "Cooperative grasping and transport using multiple quadrotors," in *Distributed Autonomous Robotic Systems*, ser. Springer Tracts in Advanced Robotics. Springer Berlin Heidelberg, 2013, vol. 83, pp. 545–558.

[2] L. Marconi, R. Naldi, and L. Gentili, "Modelling and control of a flying robot interacting with the environment," *Automatica*, vol. 47, no. 12, pp. 2571 – 2583, 2011.

[3] K. Alexis, C. Huerzeler, and R. Siegwart, "Hybrid modeling and control of a coaxial unmanned rotorcraft interacting with its environment through contact," in *2013 International Conference on Robotics and Automation (ICRA)*, Karlsruhe, Germany, 2013, pp. 5397–5404.

[4] C. Papachristos and A. Tzes, "Large object pushing via a direct longitudinally-actuated unmanned tri-tiltrotor," in *Mediterranean Conference on Control Automation (MED), 2013*, pp. 173 –178.

[5] R. Goebel, R.G. Sanfelice, and A.R. Teel, *Hybrid Dynamical Systems: Modeling, Stability, and Robustness*. 41 William Street, Princeton, NJ, USA: Princeton University Press, 2012.

[6] C. Huerzeler, "Modeling and design of unmanned rotorcraft systems for contact based inspection," Ph.D. dissertation, Swiss Federal Institute of Technology Zurich, 2013.

[7] G. B. Fabio Dabilo Torrisi, Alberto Bemporad, *HYSDEL - HYbrid System DEscription Language*, The Hybrid Systems Group, IFA–ETHZ, http://control.ee.ethz.ch/hybrid/hysdel/.

[8] M. Herceg, M. Kvasnica, C. Jones, and M. Morari, "Multi-Parametric Toolbox 3.0," in *Proc. of the European Control Conference*, Zürich, Switzerland, July 17–19 2013, pp. 502–510.

[9] K. Alexis, G. Nikolakopoulos, and A. Tzes, "Constrained-control of a quadrotor helicopter for trajectory tracking under wind-gust disturbances," in *MELECON 2010-2010 15th IEEE Mediterranean Electrotechnical Conference*. IEEE, 2010, pp. 1411–1416.

[10] K. Alexis, G. Nikolakopoulos and A. Tzes, "Model predictive quadrotor control: attitude, altitude and position experimental studies," *Control Theory & Applications, IET*, vol. 6, no. 12, pp. 1812–1827, 2012.

[11] K. Alexis and G. Nikolakopoulos and A. Tzes, "Switching model predictive attitude control for a quadrotor helicopter subject to atmospheric disturbances," *Control Engineering Practice*, 2011.

[12] C. Papachristos, K. Alexis, and A. Tzes, "Model predictive hovering–translation control of an unmanned tri–tiltrotor," in *2013 International Conference on Robotics and Automation*, Karlsruhe, Germany, 2013, pp. 5405–5412.

[13] J. Loefberg, "Yalmip : A toolbox for modeling and optimization in MATLAB," in *Proceedings of the CACSD Conference*, Taipei, Taiwan, 2004. [Online]. Available: http://users.isy.liu.se/johanl/yalmip

[14] M. Baotic, "Optimal control of piecewise affine systems," Ph.D. dissertation, Swiss Federal Institute of Technology Zurich, 2005.

[15] M. Kvasnica, *Real–Time Model Predictive Control via Multi–Parametric Programming: Theory and Tools*. VDM Verlag, 2009.

[16] M. Kvasnica, I. Rauova, and M. Fikar, "Automatic code generation for real-time implementation of model predictive control," in *Computer-Aided Control System Design (CACSD), 2010 IEEE International Symposium on*, sept. 2010, pp. 993 –998.